Understanding the Daily Cycle of Evapotranspiration: A Method to Quantify the Influence of Forcings and Feedbacks

CHIEL C. VAN HEERWAARDEN AND JORDI VILÀ-GUERAU DE ARELLANO

Meteorology and Air Quality Section, Wageningen University, Netherlands

AMANDA GOUNOU, FRANÇOISE GUICHARD, AND FLEUR COUVREUX

CNRM-GAME, Météo-France, and CNRS, Toulouse, France

(Manuscript received 13 January 2010, in final form 24 July 2010)

ABSTRACT

A method to analyze the daily cycle of evapotranspiration over land is presented. It quantifies the influence of external forcings, such as radiation and advection, and of internal feedbacks induced by boundary layer, surface layer, and land surface processes on evapotranspiration. It consists of a budget equation for evapotranspiration that is derived by combining a time derivative of the Penman–Monteith equation with a mixed-layer model for the convective boundary layer. Measurements and model results for days at two contrasting locations are analyzed using the method: midlatitudes (Cabauw, Netherlands) and semiarid (Niamey, Niger). The analysis shows that the time evolution of evapotranspiration is a complex interplay of forcings and feedbacks. Although evapotranspiration is initiated by radiation, it is significantly regulated by the atmospheric boundary layer and the land surface throughout the day. In both cases boundary layer feedbacks enhance the evapotranspiration up to 20 W m^{-2} h^{-1}. However, in the case of Niamey this is offset by the land surface feedbacks since the soil drying reaches −30 W m^{-2} h^{-1}. Remarkably, surface layer feedbacks are of negligible importance in a fully coupled system. Analysis of the boundary layer feedbacks hints at the existence of two regimes in this feedback depending on atmospheric temperature, with a gradual transition region in between the two. In the low-temperature regime specific humidity variations induced by evapotranspiration and dry-air entrainment have a strong impact on the evapotranspiration. In the high-temperature regime the impact of humidity variations is less pronounced and the effects of boundary layer feedbacks are mostly determined by temperature variations.

1. Introduction

The exchange of water between the land surface and the atmosphere is an essential component of the hydrologic cycle. Previous studies have shown that this exchange, evapotranspiration, is closely coupled to the atmosphere (e.g., Jacobs and De Bruin 1992; Betts et al. 1996; Koster et al. 2004). To be able to make credible predictions about the water balance of the earth in future climates, it is therefore fundamental to understand the driving mechanisms behind evapotranspiration and the link between the land surface and the atmospheric boundary layer (ABL).

Evapotranspiration and land–atmosphere interactions have been the subject of many studies. These studies cover a large spectrum of spatial and temporal scales and range from conceptual studies to realistic 3D modeling. Relevant examples of large-scale studies using complex models are Betts et al. (1996), who discussed the memory of soil moisture and its impact on precipitation over a longer period, or Koster et al. (2004), who used an ensemble of GCMs to investigate the response of precipitation to soil moisture change by locating the regions with the strongest land–atmosphere coupling.

Then there are studies discussing land–atmosphere coupling on a local scale. De Bruin (1983) and McNaughton

Corresponding author address: Chiel C. van Heerwaarden, Wageningen University, P.O. Box 47, 6700 AA Wageningen, Netherlands.
E-mail: chiel.vanheerwaarden@wur.nl

DOI: 10.1175/2010JHM1272.1

and Spriggs (1986) were the first to study the land surface, ABL, and free atmosphere as a coupled system. Their finding that the ABL dynamics have an important influence on the surface evaporation formed the basis for more advanced studies. These are, for instance, Brubaker and Entekhabi (1995, 1996) and Margulis and Entekhabi (2001), who made mathematical frameworks to quantify feedbacks in the coupled land–atmosphere system. Furthermore, Ek and Holtslag (2004) quantified the link between soil moisture, surface evapotranspiration, and boundary layer clouds. Recent studies discussing evapotranspiration from an atmospheric perspective are Santanello et al. (2007), who analyzed the existence of evaporation regimes as a function of soil moisture and atmospheric stability and Raupach (2000) and van Heerwaarden et al. (2009), who investigated the impact of atmospheric temperature and moisture on surface exchange and the regulation of the surface energy balance by feedbacks.

What most of these studies have in common is that they investigate the response of the integrated set of all feedback mechanisms to variations in the properties of either the land surface or the atmosphere. To our knowledge, only the studies of Brubaker and Entekhabi (1996) and Margulis and Entekhabi (2001) have provided methods to quantify the influence of individual forcings and feedbacks in the coupled land–atmosphere system on evapotranspiration. Our study focuses on evapotranspiration on the diurnal time scale and is therefore complementary to the work of Brubaker and Entekhabi. Their study aims at understanding the longer time scales involved in the heat and moisture budget, which can for instance be seen in their assumption of a constant ABL height. In turn, we are mostly interested in time scales of one day and shorter and focus particularly on the dynamics of the ABL. The study of Margulis and Entekhabi (2001) covers a theoretical overview of the feedback pathways that exist in the land–atmosphere system on a diurnal time scale using an example based on the First International Satellite Land Surface Climatology Project (ISLSCP) Field Experiment (FIFE) data (Sellers et al. 1992) and shows in a conceptual way how studying evapotranspiration using offline models can be misleading.

In this paper, we describe a method for quantifying forcings and feedbacks during daytime convective conditions and apply it to two real data cases. In comparison to Margulis and Entekhabi (2001) our method is designed to quantify forcings and feedbacks directly from measurement or model data and is therefore complementary to their method.

The evapotranspiration is dependent on both the properties of the atmospheric boundary layer and the land surface. The temperature and humidity of the atmosphere control the maximum amount of water that the atmosphere can take up, which is the potential evapotranspiration. The land surface properties, such as vegetation characteristics and soil texture and its moisture content, determine the supply of water, thus to which degree the evapotranspiration rate reaches the potential. In the coupled land–atmosphere system, all variables are connected through a set of feedback mechanisms (Brubaker and Entekhabi 1995; van Heerwaarden et al. 2009). For instance, an increase in soil moisture results in a larger evapotranspiration rate, which in turn has a positive effect on the atmospheric moisture content and a negative effect on the temperature as less energy is available for the sensible heat flux. In section 2a we give a comprehensive description of the coupled land–atmosphere system, in which we define what we consider the forcings and the feedbacks that act on surface evapotranspiration.

The Penman–Monteith equation (Monteith 1965) provides a way to quantify surface evapotranspiration by taking into account the capacity of the atmosphere to take up water, as well as the ability of the land surface to provide it. For this reason, it is the most widely used parameterization for evapotranspiration in atmospheric and hydrologic models. In this paper we show that, by differentiating the Penman–Monteith equation with respect to time, we obtain a budget equation for evapotranspiration. This can be rewritten in a form that provides separate terms for all forcings and feedbacks that act on the evapotranspiration if it is combined with the mixed layer equations (Lilly 1968; Tennekes 1973) that describe the most essential dynamics of the daytime ABL. In section 2b we explain this budget equation in detail.

Then, we demonstrate how our method can be used to analyze data to be able to identify the driving forces behind the daily cycle of evapotranspiration. Here, we use data of two contrasting locations. The two selected cases are 25 September 2003 at Cabauw, Netherlands (Casso-Torralba et al. 2008), and 22 June 2006 at Niamey, Niger, measured during the African Monsoon Multidisciplinary Analyses (AMMA) campaign (Redelsperger et al. 2006). The first case is a typical midlatitude case, where evapotranspiration is energy limited. This case is characterized by relatively cold temperatures, a moist and fully grass-covered land surface, and only little advection. The second case corresponds to semiarid conditions, where evapotranspiration is limited by the amount of available water. This case is a hot premonsoon day over a sparsely vegetated savanna, subjected to strong heat and moisture advection in the morning and a fast-drying land surface throughout the day.

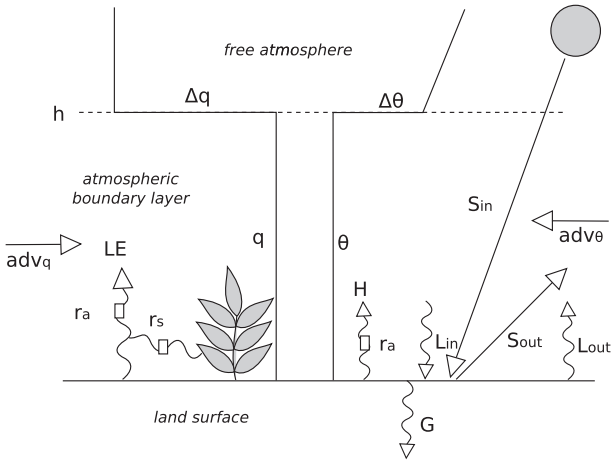

FIG. 1. Overview of the coupled land–atmosphere system and the relevant variables in the daily evolution of evapotranspiration.

We reproduce the two days using a coupled land–atmosphere model. First, in section 3 we discuss the model and the modeling experiment in detail and describe the data that we use for the model evaluation. Second, in section 4a we evaluate the model output against observations. In the subsequent analysis in section 4b we apply our budget equation to the model result and do a thorough evaluation of all the terms in the budget equation. Per location we demonstrate how our method can be used to find out the importance of the forcings compared to the feedbacks in determining to what extent the evaporation is locally regulated. In this analysis, we compare the forcings, boundary layer, and land surface feedbacks in detail.

2. Evapotranspiration analysis framework

a. Overview of the coupled land–atmosphere system

In this section we explain the elements of the coupled land–atmosphere system that are relevant for the daily evolution of evapotranspiration. Figure 1 shows all variables contained in this system and which will later appear in the budget equation presented in section 2b.

The system essentially consists of three components. First, there is the land surface, which provides water and heat to the atmosphere through the surface evapotranspiration LE and the sensible heat flux H. The energy that is available for these two processes is the net radiation Q_*, which is the sum of incoming S_{in} and outgoing S_{out} shortwave radiation and incoming L_{in} and outgoing L_{out} longwave radiation, minus the energy that enters the soil through the ground heat flux G. Land surface properties, such as the vegetation type and cover or soil moisture, are accounted for in the surface resistance r_s, whereas the turbulent characteristics of the near-surface atmosphere, which determine how efficient water is taken up, are accounted for in the aerodynamic resistance r_a.

Second, there is the convective atmospheric boundary layer that has a well-mixed profile for potential temperature θ and specific humidity q. In this layer, the moisture that enters the ABL through the surface heat fluxes and the entrainment heat fluxes is vertically mixed by convection. Large-scale temperature adv_θ and moisture adv_q advection act on the thermodynamic state of the ABL, which subsequently feeds back on the surface evapotranspiration.

Third and last, there is the free atmosphere. Its potential temperature and specific humidity minus the values in the ABL define the jumps of potential temperature $\Delta\theta$ and specific humidity Δq. These jumps are strongly related to the vertical profiles of temperature and humidity in the free troposphere [see Eqs. (A9) and (A10)]. The first determines to a large extent the ABL growth, thus the evolution of the ABL height h, whereas the latter determines the amount of dry air that can be entrained during growth of the ABL.

In this study, we strictly separate forcings and feedbacks. As forcings, we consider all processes that influence surface evapotranspiration but are not, or only very weakly, influenced by the state of the coupled land–atmosphere system on the time scale of 1 day. Therefore, these processes do not respond to the surface evapotranspiration; thus we assume them to be external forcings. As feedbacks on surface evapotranspiration, we consider the processes that react on the surface evapotranspiration and, because of this reaction, have an influence on the evapotranspiration itself. Because these processes locally regulate the evapotranspiration, we call them feedbacks. In the next section we discuss the complete set of forcings and feedbacks in the system.

b. Budget equation for surface evapotranspiration

Now, we introduce the mathematical expression that describes the time evolution of evapotranspiration LE as a function of all forcings and feedbacks in the coupled land–atmosphere system, sketched in Fig. 1. This equation is acquired by combining a time derivative of the Penman–Monteith equation with the mixed-layer equations for the ABL (see appendix A for a full derivation). Equations (1) and (2) show the tendency of evapotranspiration ordered in forcings and feedbacks:

$$\frac{dLE}{dt} = \overbrace{c_0 \frac{dq_{\mathrm{sat}}}{dT}\left\{(1-\alpha)\frac{dS_{\mathrm{in}}}{dt} + \frac{dL_{\mathrm{in}}}{dt}\right\}}^{\text{surface radiation forcing}} + \overbrace{c_0\left(H\frac{d^2q_{\mathrm{sat}}}{dT^2} + \frac{\rho c_p}{r_a}\frac{dq_{\mathrm{sat}}}{dT}\right)\{\mathrm{adv}_\theta\} - c_0\frac{\rho c_p}{r_a}\{\mathrm{adv}_q\}}^{\text{boundary-layer forcings}}$$
$$+ \overbrace{c_0\left(H\frac{d^2q_{\mathrm{sat}}}{dT^2} + \frac{\rho c_p}{r_a}\frac{dq_{\mathrm{sat}}}{dT}\right)\left\{\frac{H}{\rho c_p h} + \frac{w_e\Delta\theta}{h}\right\} - c_0\frac{\rho c_p}{r_a}\left\{\frac{LE}{\rho L_v h} + \frac{w_e\Delta q}{h}\right\}}^{\text{boundary-layer feedbacks}} - \overbrace{c_0\left(\frac{\rho c_p}{r_a^2}(q_{\mathrm{sat}} - q) - LE\frac{c_p}{L_v}\frac{r_s}{r_a^2}\right)\frac{dr_a}{dt}}^{\text{surface-layer feedback}}$$
$$- \overbrace{c_0\frac{dq_{\mathrm{sat}}}{dT}\frac{dL_{\mathrm{out}}}{dt} - c_0\frac{dq_{\mathrm{sat}}}{dT}\frac{dG}{dt} - c_0 LE\frac{c_p}{L_v}\frac{1}{r_a}\frac{dr_s}{dt}}^{\text{land surface feedbacks}}, \quad (1)$$

$$c_0 = 1\Big/\left[\frac{dq_{\mathrm{sat}}}{dT} + \frac{c_p}{L_v}\left(1 + \frac{r_s}{r_a}\right)\right] \quad (2)$$

in which dq_{sat}/dT is the change of saturated specific humidity with respect to temperature, c_p the heat capacity of air at constant pressure, L_v ithe latent heat of vaporization, ρ the density of the atmosphere, w_e the entrainment velocity, and α is the albedo of the land surface.

Each of the terms on the right-hand side shows the contribution of a separate process to the time evolution of evapotranspiration. The terms can be interpreted as a sensitivity of evapotranspiration to a change in a variable $\partial LE/\partial \mathrm{var}$ multiplied with the tendency of that specific variable $d\mathrm{var}/dt$, although in the case of potential temperature and specific humidity, the tendency has been replaced by the mixed-layer equations (see appendix A). The five lines, in which the terms are ordered in their respective category, represent the following:

1) *Surface radiation forcing.* This forcing represents the effects of variations in the incoming radiation. The first term represents the net shortwave radiation, since the outgoing shortwave is defined as the albedo α multiplied by S_{in}, whereas the second term represents the incoming longwave radiation. Both are considered as external forcings. The net shortwave radiation represents the incoming solar energy, and, since we do not take clouds into account here, it is therefore independent of the properties of the coupled land–atmosphere system. Although the incoming longwave radiation is function of the atmospheric temperature, it is rather insensitive to fluctuations in the ABL temperature on the time scale of 1 day and is therefore assumed to be an external forcing. Both terms are positively related to the evapotranspiration tendency, for the reason that more available energy allows for more evapotranspiration.
2) *Boundary layer forcing.* This forcing represents the large-scale processes that influence either the potential temperature or the specific humidity of the mixed layer. In this study, where we do not consider clouds or radiation divergence in the atmosphere, this is only the large-scale advection. The first term describes the potential temperature advection. The second term represents the consequences of large-scale moisture advection. The boundary layer forcings and feedbacks, shown in the next paragraph, enhance evapotranspiration if they warm or dry the ABL and reduce evapotranspiration if they cool or moisten the ABL.
3) *Boundary layer feedbacks.* The first term of this forcing represents the effects of the surface (first term in bracket) and entrainment (second term in bracket) sensible heat flux on the potential temperature. The second term of this forcing describes the impact of evapotranspiration (first term in bracket) and dry-air entrainment (second term in bracket) on the specific humidity.
4) *Surface-layer feedbacks.* This term represents the impact of changes in the atmospheric resistance. If the atmosphere becomes more unstable or if the surface wind speed increases, then the atmospheric resistance decreases and evapotranspiration rises.
5) *Land surface feedbacks.* This last term shows the effects of the three processes of which the land surface feedbacks consist. The first term represents the outgoing longwave radiation, which is a function of the surface temperature. The second term describes the ground heat flux, which is the part of the incoming radiation that enters the ground and is therefore not available for evapotranspiration. The third term accounts for variations in the surface resistance, which are induced by the response of the vegetation to changes in radiation or soil moisture or by the drying of the soil in the case of bare soil evaporation. An increase in outgoing longwave radiation results in a reduction of the evapotranspiration because it reduces the net radiation. Similarly, a rise in the ground heat flux results in a decrease of evapotranspiration as this reduces the available net radiation. An increase in surface resistance results in a fall

in evapotranspiration as the land surface is less efficient in making water available for evapotranspiration.

3. Methods

a. Model

Here, we define the experiment to which we apply our framework. We use an extended version of the simple coupled land–atmosphere model described in van Heerwaarden et al. (2009). This model is inspired by the early studies of De Bruin (1983) and McNaughton and Spriggs (1986) and has proven to be successful in reproducing the essential land–atmosphere feedbacks accurately. The atmospheric part of the model is described in appendix A by Eqs. (A5) to (A10) and is based on Lilly (1968) and Tennekes (1973). We have extended these models by including a simple radiation model, dynamical models for the aerodynamic and surface resistance, and a soil model.

In the simple radiation model the incoming shortwave radiation is a function of the time, day, latitude, and longitude and the incoming longwave radiation a function of the mixed-layer temperature.

To calculate the atmospheric resistance we include stability corrections based on Monin–Obukhov similarity theory, using the integrated flux–gradient relationship as proposed by Paulson (1970). For this, we evaluate the gradient at the top of the surface layer, assuming that this height is at 0.1 of the boundary layer height calculated by the atmospheric model.

To mathematically describe the land surface and be able to model partially vegetated surfaces, we have introduced a force–restore soil model. The surface energy balance and temperature equations are based on Duynkerke (1991), whereas the soil moisture equations are based on Noilhan and Planton (1989). We chose the soil temperature description of Duynkerke (1991) over that of Noilhan and Planton (1989) since this formulation yields more accurate ground heat fluxes for nearly fully vegetated surfaces, as in Cabauw. Since, in contrast to van Heerwaarden et al. (2009), we have added a soil model, the ground heat flux is resolved and therefore no longer a fixed fraction of the net radiation.

The evapotranspiration calculated by the model is a sum of three components: transpiration from vegetation, evaporation from bare soil, and evaporation from wet foliage. A bulk surface resistance r_s is diagnosed from this sum and used in our budget equation for evapotranspiration. The computation of the transpiration from vegetation requires a canopy resistance, which we compute using the Jarvis–Stewart model [Jarvis (1976), see appendix B for a full description]. We added a parameterization to take into account the impact of the interception water and dew formation on evapotranspiration (Viterbo and Beljaars 1995).

b. Numerical experiments

1) CABAUW, NETHERLANDS: 25 SEPTEMBER 2003

For our first case, we have selected measurements from Cabauw, Netherlands, observed during 25 September 2003 (Casso-Torralba et al. 2008). This was a cloudless day with negligible horizontal advection for heat and moisture. The early morning profile was characterized by a large and moist residual layer, which had a very strong inversion on top of it above which the atmosphere was relatively dry. In appendix C we have included a list of all model parameters, initial conditions, and boundary conditions for this study.

To evaluate our model results, we use tower measurements of temperature and dewpoint temperature taken at 140 m to calculate the mixed-layer temperature θ and the mixed-layer specific humidity q. In addition, we compare surface measurements of incoming and outgoing shortwave and longwave radiation with the radiation balance calculated by the model. Furthermore, we evaluate the calculated surface sensible H and latent LE heat flux against 10-min eddy correlation data, measured at 3 m above the land surface. The calculated atmospheric boundary layer height h is evaluated against low-mode wind profiler measurements.

2) NIAMEY, NIGER: 22 JUNE 2006

For the second case, we have selected 22 June 2006 measured during the AMMA campaign (Redelsperger et al. 2006). This was a nearly cloudless day in the early stage of the monsoon. Deep convection with heavy rainfall occurred during the previous night, which provided water to the soil. A large part of this water was already removed via runoff, drainage, or evaporation during the night. There is a large diurnal cycle of temperature combined with a strong drying of the soil throughout the day. In addition, both the moisture and the temperature balance are significantly affected by advection of relatively moist and cold air, which ceases in the afternoon.

To validate the model, we use surface measurements of the Atmospheric Radiation Measurement Program (ARM) mobile facility (Miller and Slingo 2007), which measured the surface energy and radiation balance at the location. The mixed-layer potential temperature θ and specific humidity q are validated by comparing them to four radiosoundings taken at intervals of 3 h. From these radiosoundings, the boundary layer height h is constructed by picking the lowest height at which the

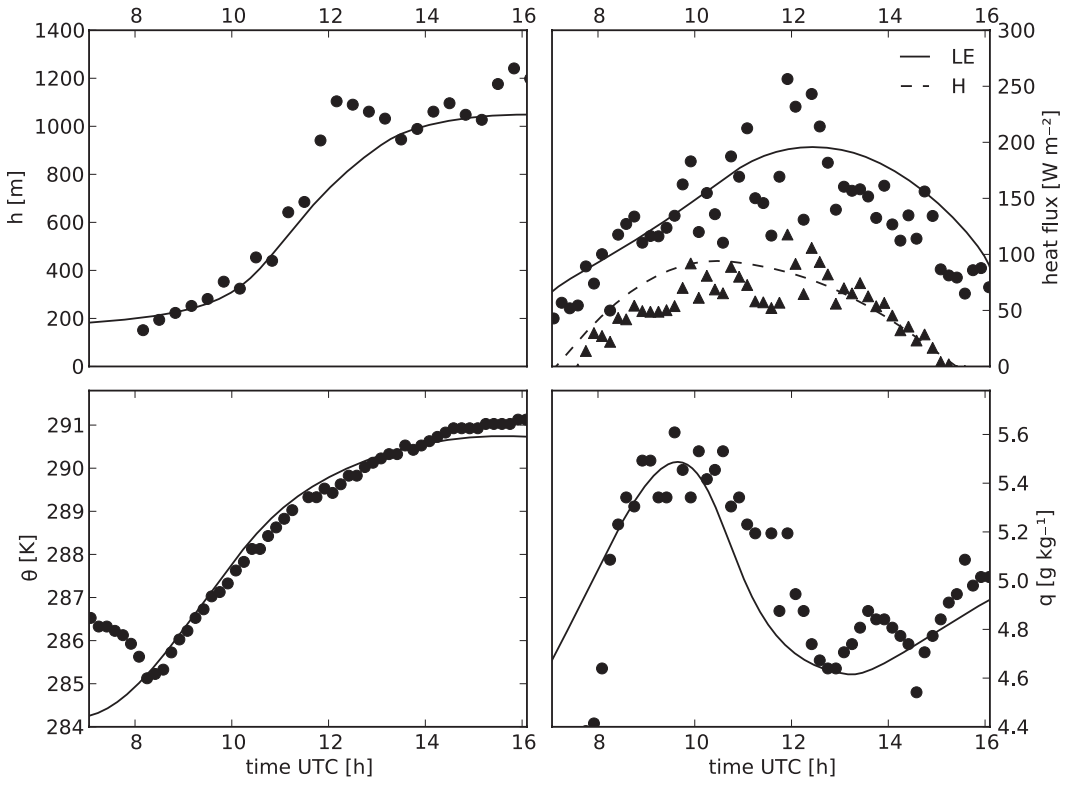

FIG. 2. Time evolution of (top left) boundary layer height, (top right) surface heat fluxes, (bottom left) potential temperature of the mixed layer, and (bottom right) specific humidity of the mixed layer for the Cabauw case. The model is represented by continuous lines, observations by symbols.

virtual potential temperature at that specific height is 0.25 K higher than the mean from the land surface to that height. The mixed-layer potential temperature and humidity are acquired by averaging the radiosounding from the land surface to the boundary layer height. The turbulent fluxes of temperature and moisture that represent the sensible H and latent LE heat flux are compared with eddy correlation measurements taken at the airport of Niamey, where the vegetated part of the land surface is covered with grass. Initial soil temperatures are close to those measured at the nearby station of Wankama. Large-scale advection tendencies are estimated from the ECMWF reanalysis data for the AMMA observational campaign.

4. Results

a. Model validation

1) CABAUW, NETHERLANDS

We start our analysis by verifying the capability of the model to reproduce the measurements of the selected case of 25 September 2003. First, we compare the measured and modeled radiation balance, which confirms a close match between the model and the observations (not shown). Second, we validate the model against the measured potential temperature, specific humidity, boundary layer height, and surface heat fluxes (see Fig. 2).

Here, we find a satisfactory agreement between the measured and modeled boundary layer height, potential temperature, and specific humidity, which is a confirmation that our conceptual model captures the most relevant dynamics of the coupled land–atmosphere system. The data of the boundary layer height shows significant fluctuations in the afternoon, which could be related to the measurement error in this data, which could reach 40% (Steeneveld et al. 2007). Nevertheless, the fact that our model reproduces the time evolution of the specific humidity well is an indication that the complex interplay of surface and entrainment fluxes is correctly represented by the model. Note that between 0730 and 0810 UTC the modeled potential temperature and specific humidity deviate strongly from the measurements. In the early morning phase, the ABL is not yet well mixed, whereas within our model setup we assume it to be. This causes a deviation from the observations that quickly disappears after 0800 UTC when the ABL becomes well mixed.

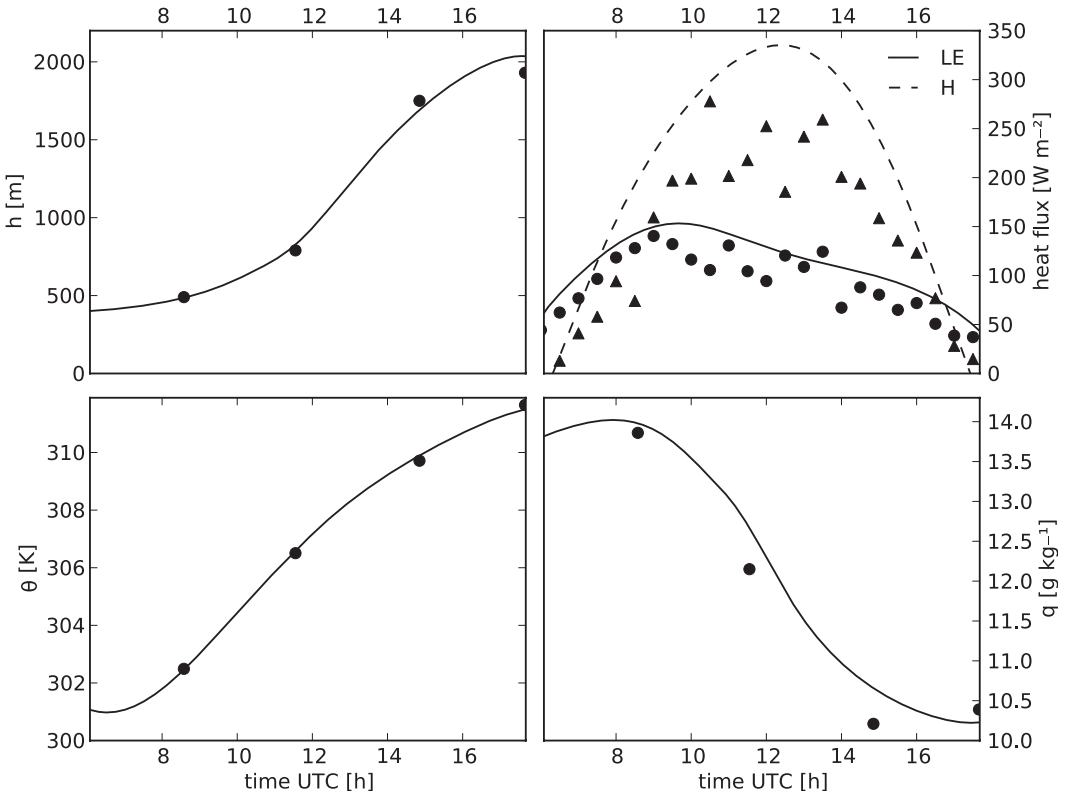

FIG. 3. As in Fig. 2 but for Niamey.

The modeled surface heat fluxes show larger differences with the observed data than the temperature and humidity, although they approximately capture the values and tendencies. Since closing the surface energy balance is notoriously difficult using eddy covariance data (Brotzge and Crawford 2003) and the tower has a different footprint than the surface flux measurements, we assume that the correct reproduction of the boundary layer properties confirms that we model the appropriate fluxes.

2) NIAMEY, NIGER

Also for the second case, the model compares well with the measurements. There is a close match between the measured and modeled radiation at the surface, which confirms that we prescribe the right available energy to the model (not shown). In addition, the modeled surface heat fluxes and the height, temperature, and humidity of the mixed layer match well with the observations (see Fig. 3). This is confirmed by a comparison of the mixed-layer profiles with radiosoundings taken at 3-h intervals during this day, shown in Fig. 4. The figure proves the quality of the mixed-layer model in convective conditions. The potential temperature and the specific humidity are described well over the whole mixed-layer depth by a single value. Only in the profile at 1740 UTC, a limited gradient is observed in the top of the mixed layer for both temperature and moisture. At this time the virtual heat flux at the surface is barely positive anymore (see Fig. 3) and the mixing is therefore less intense.

The surface evapotranspiration measurements show a good match with the modeled evapotranspiration, but the modeled values are slightly higher than the observations. Since the curve describing the modeled evapotranspiration follows the complex tendency of the observations well, we can assume that both of the processes at the land surface and in the atmosphere are adequately reproduced by the model. The fact that a large part of the rainwater already left the system during the night, explains the fast decline of evapotranspiration during the day as the reservoir is quickly depleted. The sensible heat flux is, similar to the evapotranspiration, greater in the model results than in the observations. Under the conditions at Niamey, a nonclosure of the surface energy balance up to 20% of the net radiation is very common (Ramier et al. 2009). In our case, this would indicate a loss of approximately 100 W m^{-2}, which is more than the difference between the modeled

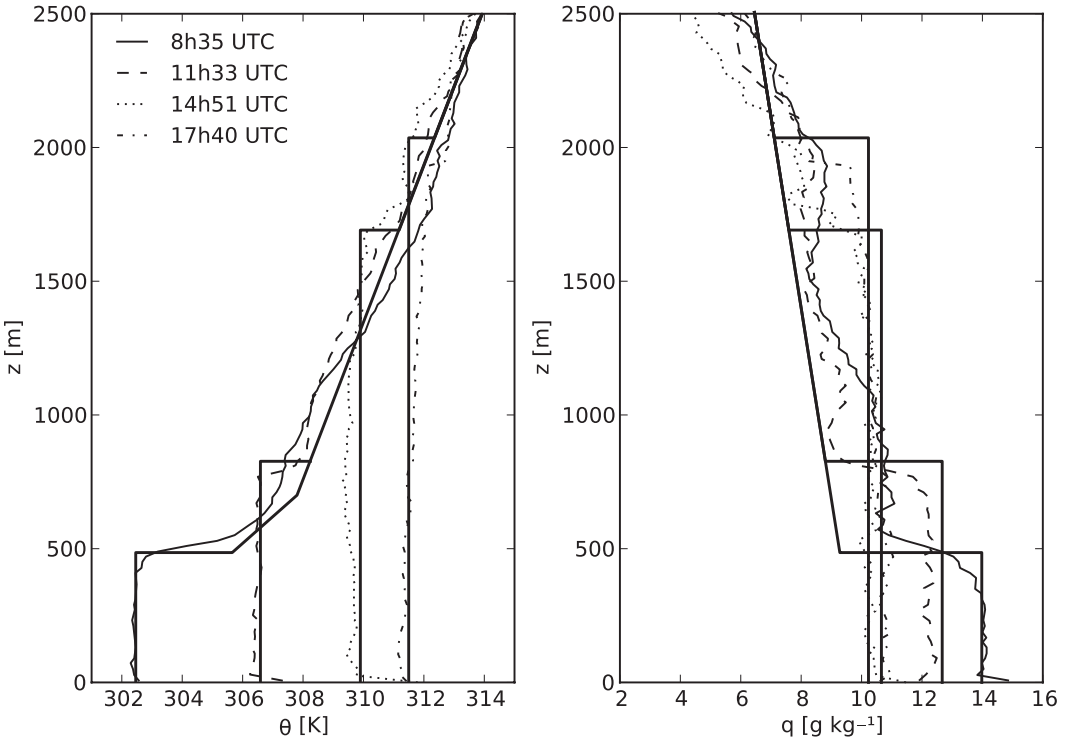

FIG. 4. Comparison between radiosoundings (thin line) and model results (thick line) for (left) potential temperature and (right) specific humidity at Niamey.

and observed surface fluxes. Since we are able to reproduce the radiosoundings, we assume that the modeled surface heat fluxes are representative for our case.

To conclude, the land–atmosphere model is able to reproduce the most important boundary layer and surface flux characteristics of the two selected cases, therefore validating the application of the model output data as input for our evapotranspiration analysis framework.

b. Analysis of the daily cycle of evapotranspiration

1) OVERVIEW OF FORCINGS AND FEEDBACKS

We start the analysis of evapotranspiration by showing in Fig. 5 an overview of the total tendency of evapotranspiration and the separate contribution of the five categories of forcings and feedbacks defined in Eq. (1).

According to the figure, there are strong similarities as well as differences between the two cases. In both cases, the surface radiation forcing is the main external driver of the system. It contributes positively in the morning when the sun rises fast, adding more than 30 W m^{-2} h^{-1} to the evapotranspiration. Then, at 1140 UTC at Cabauw and at 1200 UTC at Niamey it crosses the zero line, marking the position of the sun closest to the zenith, and during the remainder of the day the contribution becomes more negative as the angle between the sun and the zenith increases again. In Cabauw, the surface radiation forcings decrease linearly over the majority of the day, whereas in Niamey, the slope of the line representing the forcing is less negative in the afternoon than in the morning, thus radiation is less effective in influencing the surface evapotranspiration later during the day. It is also found that the impact of heat and moisture advection on evapotranspiration is minimal in Niamey. In section 4, we will explain these findings after an in-depth analysis of the forcings.

Despite the similarities in the surface radiation forcings, there is a large difference in the time evolution of the evapotranspiration tendency of the two cases. A first explanation is that in Cabauw the three feedbacks (see Figs. 5c,d) add up to a positive tendency during the majority of the day, whereas in Niamey they add up to negative values most of the day. The differences in the feedbacks can also be found in the plot showing the forcings (see Figs. 5a,b). In the case of Cabauw, the total tendency is larger than the tendency induced by the forcings during the period from 0900 to 1400 UTC, which implies that the feedbacks enhance evapotranspiration. The case for Niamey shows the opposite. Here, the total tendency is less than the tendency induced by the forcings alone until 1400 UTC. Therefore, the impact of the feedbacks must be negative most of the day.

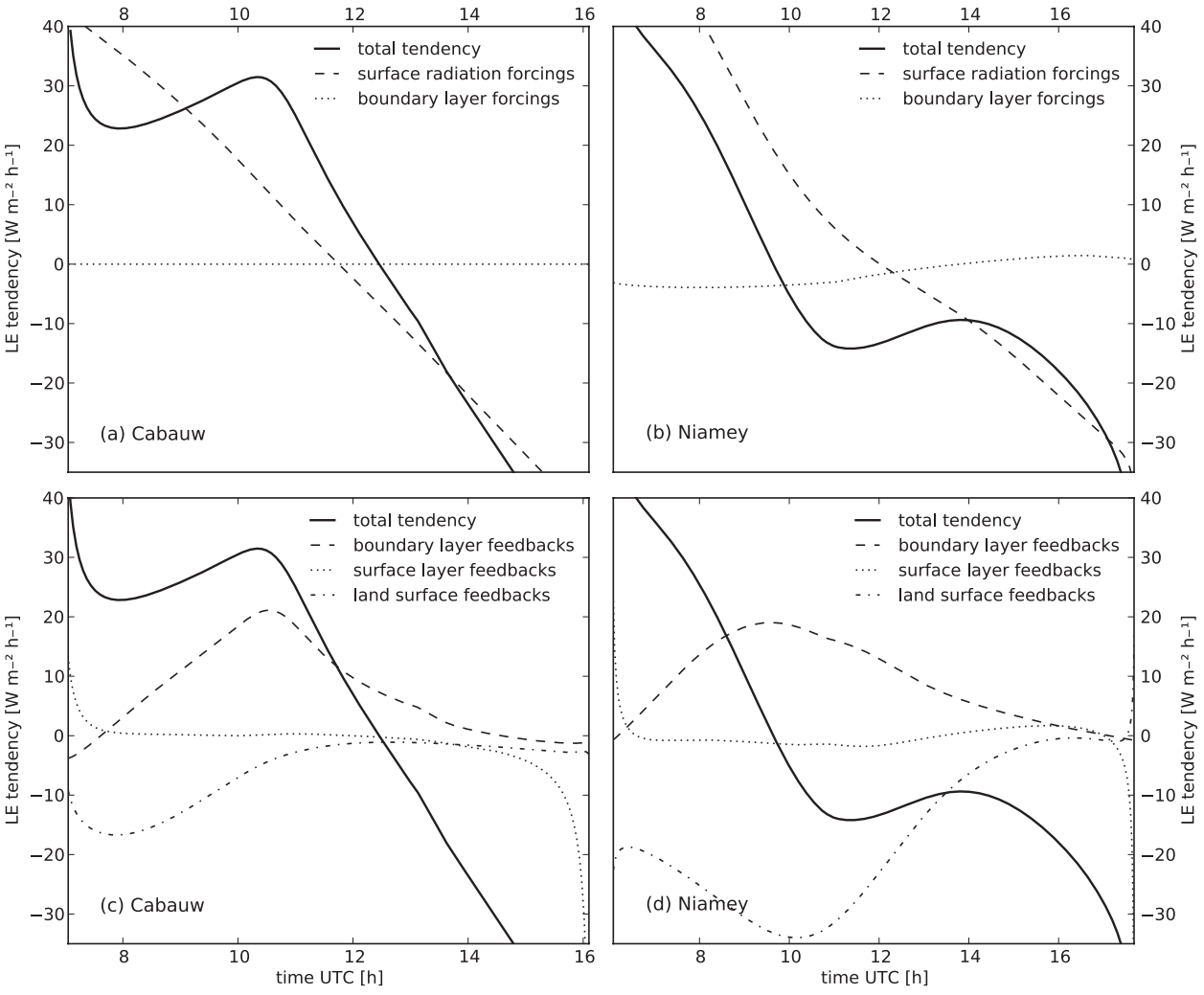

FIG. 5. Contributions to the tendency of the surface evaporation induced by (top) forcings and (bottom) feedbacks for (left) Cabauw and (right) Niamey.

The cause for the large difference between the cases can be found in the land surface feedbacks. At Cabauw, the land surface feedback has only a modest negative impact in the morning with a minimum of -17 W m^{-2} h^{-1} at 0800 UTC. Thereafter, its value quickly rises and after 1200 UTC its contribution is negligible. At Niamey we find a much larger negative impact, reaching -35 W m^{-2} h^{-1} just after 1000 UTC and remaining significantly negative until 1600 UTC. In section 4b(2) we elaborate on the land surface feedbacks in the two cases and discuss the differences in the driving mechanisms to explain this large difference.

In contrast to the land surface feedbacks, the contribution of the boundary layer feedbacks is comparable between the two cases. Both have a rising contribution in the morning, with a peak near 1000 UTC of 20 W m^{-2} h^{-1} and are thereafter gradually reducing toward zero. The similarity between the two cases is striking, as there is a large difference in the partitioning of the surface fluxes and in the related time evolution of the ABL properties (see Figs. 2 and 3). In section 4b(3) we discuss the boundary layer feedbacks in detail.

In both cases, the surface-layer feedback is of low importance throughout the majority of the day. Its contribution is large only in the early morning at the onset of convection and in the evening transitions when convection stops. The weak influence of surface layer feedbacks is because the relative changes in the aerodynamic resistance are small, as the resistance is strongly buffered in the coupled system. This is caused by the inverse relationship between the drag coefficient and wind, from which r_a is computed: $r_a = (C_D U)^{-1}$. This relation implies that, if wind speed increases, the surface layer becomes less unstable, thus C_D decreases and vice versa.

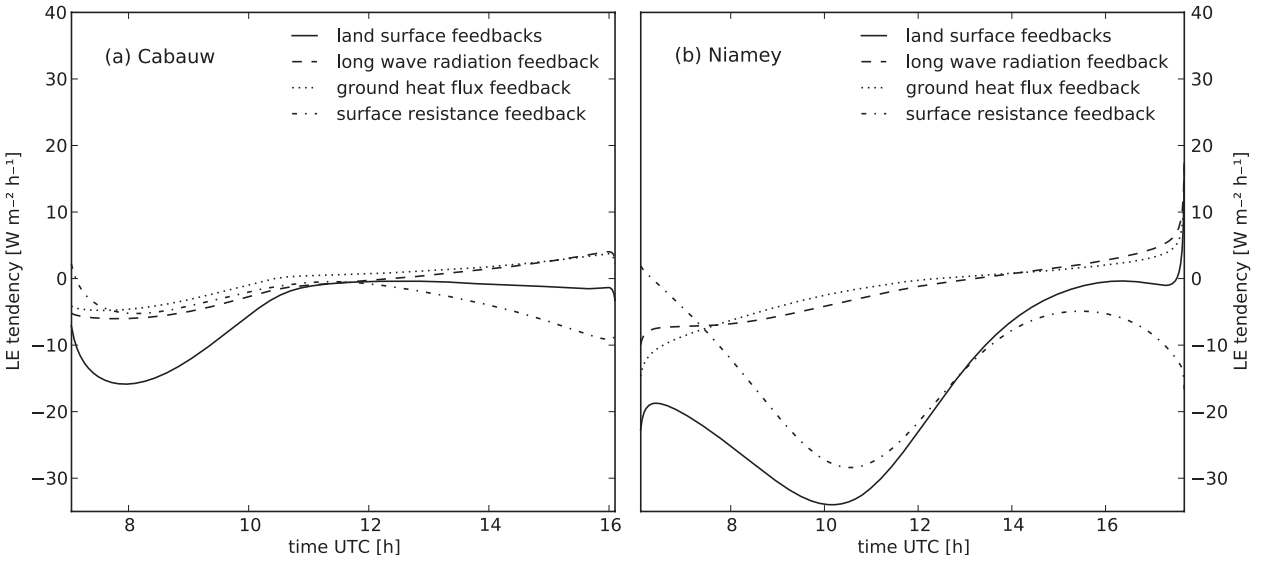

FIG. 6. Contributions of land surface feedbacks to the tendency of the surface evaporation for (left) Cabauw and (right) Niamey.

The irrelevance of the surface layer feedback confirms the findings of McNaughton and Spriggs (1986), who found that in coupled models the evapotranspiration is insensitive to aerodynamic resistance.

To summarize, we have three open questions now, which we will answer by analyzing the boundary layer feedbacks, land surface feedbacks, and forcings in detail using our method. First, we analyze what drives the land surfaces feedbacks at both locations. Second, we explain why the boundary layer feedbacks are so similar in both cases, despite the striking differences between them. Third, we explain why the radiation forcing is less efficient in the afternoon at Niamey, while it retains its strength at Cabauw and why the impact of advection is so small for Niamey.

2) LAND SURFACE FEEDBACKS

In Fig. 6 we show the land surface feedbacks, decomposed into the three terms in Eq. (1), which are related to the outgoing longwave radiation, the ground heat flux, and the surface resistance. The evolution of the surface resistance feedback makes the large difference between the two cases, having only little dynamics at Cabauw in contrast to a large diurnal cycle over Niamey. At Cabauw the contribution is slightly negative throughout the day with a minimum of -5 W m^{-2} h^{-1} at 0800 UTC, then rising slightly toward 0 W m^{-2} h^{-1} near 1100 UTC, and thereafter gradually falling to -10 W m^{-2} h^{-1} in the evening transition when convection stops. In the morning there is dew on the leaves, which makes evaporation at the potential rate possible for a limited fraction of the vegetation. The dew water reservoir is depleted quickly and the surface resistance consequently rises, thus explaining the modest peak at 0800 UTC. The gradually increasing negative impact in the afternoon is explained by the response of the plants to the fall in shortwave radiation. The time evolution of the surface variables at Cabauw (see Fig. 7) demonstrates the modest temperature range and the limited increase of the surface resistance in the morning.

At Niamey, the surface resistance feedback falls to -28 W m^{-2} h^{-1} from the moment that convection starts until 1030 UTC. Afterward, the impact of the feedbacks decreases considerably, reaching a maximum of -8 W m^{-2} h^{-1} at 1520 UTC but falls thereafter again. Over Niamey, the majority of the evapotranspiration is bare soil evaporation. Since there has been precipitation during the night, the day starts with moist soil. First, the evapotranspiration is rising (see Fig. 3), thereby depleting the soil moisture at an increasing rate and progressively increasing the surface resistance. Note that, despite the fast increase of the resistance, the evapotranspiration is initially still rising because the forcings and boundary layer feedback compensate for it (see Fig. 5). This phase is pointed out by Brubaker and Entekhabi (1995), who show that anomalies in soil moisture are reinforced by a rise in surface temperature. This rise can be found in Fig. 7 that shows the time evolution of surface and soil temperature.

After reaching the evapotranspiration peak just before 1000 UTC, the water in the top soil layer is depleted. Although the resistance increases at a high pace (see Fig. 7), the increase of large resistances to even

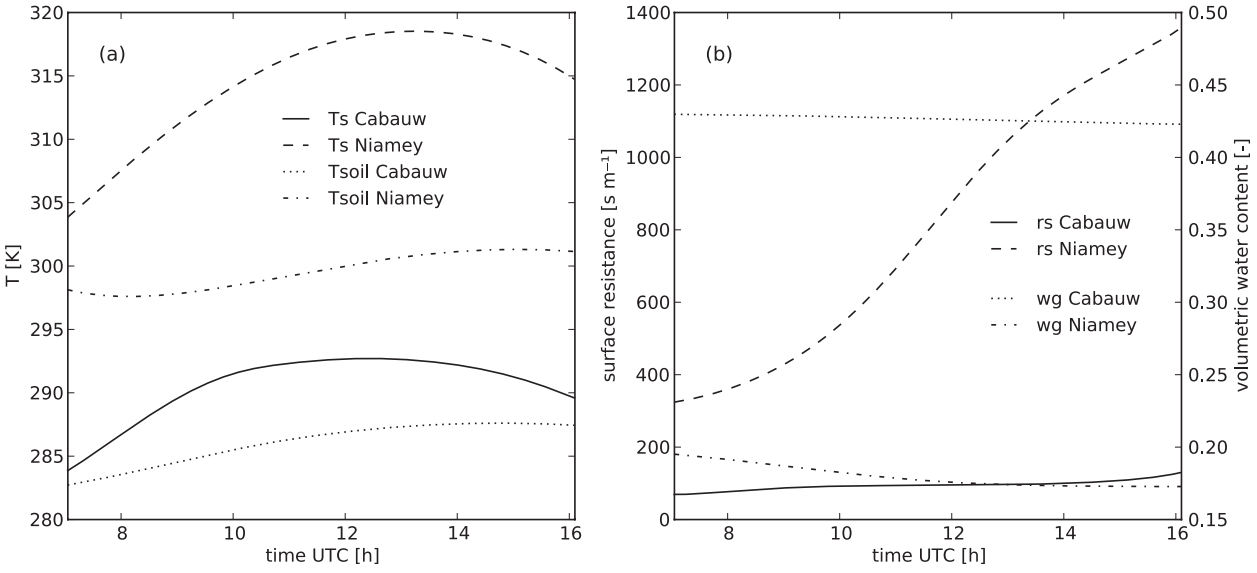

FIG. 7. Time evolution of (left) surface temperature and soil temperature and (right) surface resistance and soil volumetric water content for both cases.

larger resistances only has a limited effect on the evapotranspiration. Therefore, the contribution of the surface resistance to the evapotranspiration tendency becomes less negative in time.

The contributions of longwave radiation and the ground heat flux to the land surface feedbacks are similar for the two cases, slightly negative in the morning (-5 W m^{-2} h^{-1} for Cabauw and -10 W m^{-2} h^{-1} for Niamey) and almost linearly increasing throughout the day, changing to positive around noon. Both feedbacks are inversely related to the incoming radiation. If the incoming radiation increases, the surface temperature rises. This means that more energy enters the soil through the ground heat flux and more of the incoming radiation leaves the surface via outgoing longwave radiation. Consequently, there is a negative impact on evapotranspiration. Shortly after the sun reaches its smallest angle to the zenith, the surface temperature starts decreasing, and both contributions become positive because the decrease in soil heat flux and outgoing longwave radiation makes more energy available for evapotranspiration. The amplitude of these two contributions is larger at Niamey compared to Cabauw because of the larger diurnal range of surface temperatures.

3) BOUNDARY LAYER FEEDBACKS

Here, we compare in detail the boundary layer feedbacks of the two cases. To quantify the relevance of each individual boundary layer process, we calculate the four components of the boundary layer feedbacks shown in Eq. (1) (see Fig. 8).

Although we concluded in the previous analyses that there is a similar total contribution of the boundary layer feedbacks between the two cases, there is considerable difference in the magnitude of the four terms that add up to the total. At Cabauw the boundary layer feedbacks are just as much influenced by the temperature-related processes as the moisture-related processes. In the morning, when the boundary layer is warming fast between 0900 and 1000 UTC, the increase of temperature by surface heating has a positive contribution to evapotranspiration close to 10 W m^{-2} h^{-1}. This positive enhancement is more than compensated by the decrease of the evapotranspiration caused by the moistening of the air, which is close to -10 W m^{-2} h^{-1} until 1000 UTC. Later during the day, the effects of the surface heat fluxes decrease due to boundary layer growth: now the surface fluxes enter a larger reservoir, that is, the fully developed ABL, and therefore require more time to modify the atmospheric temperature or specific humidity.

The effect of entrainment is well pronounced. Especially the effect of dry-air entrainment, at 1040 UTC, has a strong positive contribution to the surface evapotranspiration of 15 W m^{-2} h^{-1}. At this time the boundary layer grows fastest and is still relatively moist (see Fig. 2). The quick drop of specific humidity (from 5.5 to 4.6 g kg^{-1}), occurring then, has a strong influence on the moisture deficit and, thus, on evapotranspiration. The effect of temperature entrainment also contributes significantly to the surface evapotranspiration. The distinct peak that we find in moisture is, however, absent, because temperature entrainment fluctuates less throughout

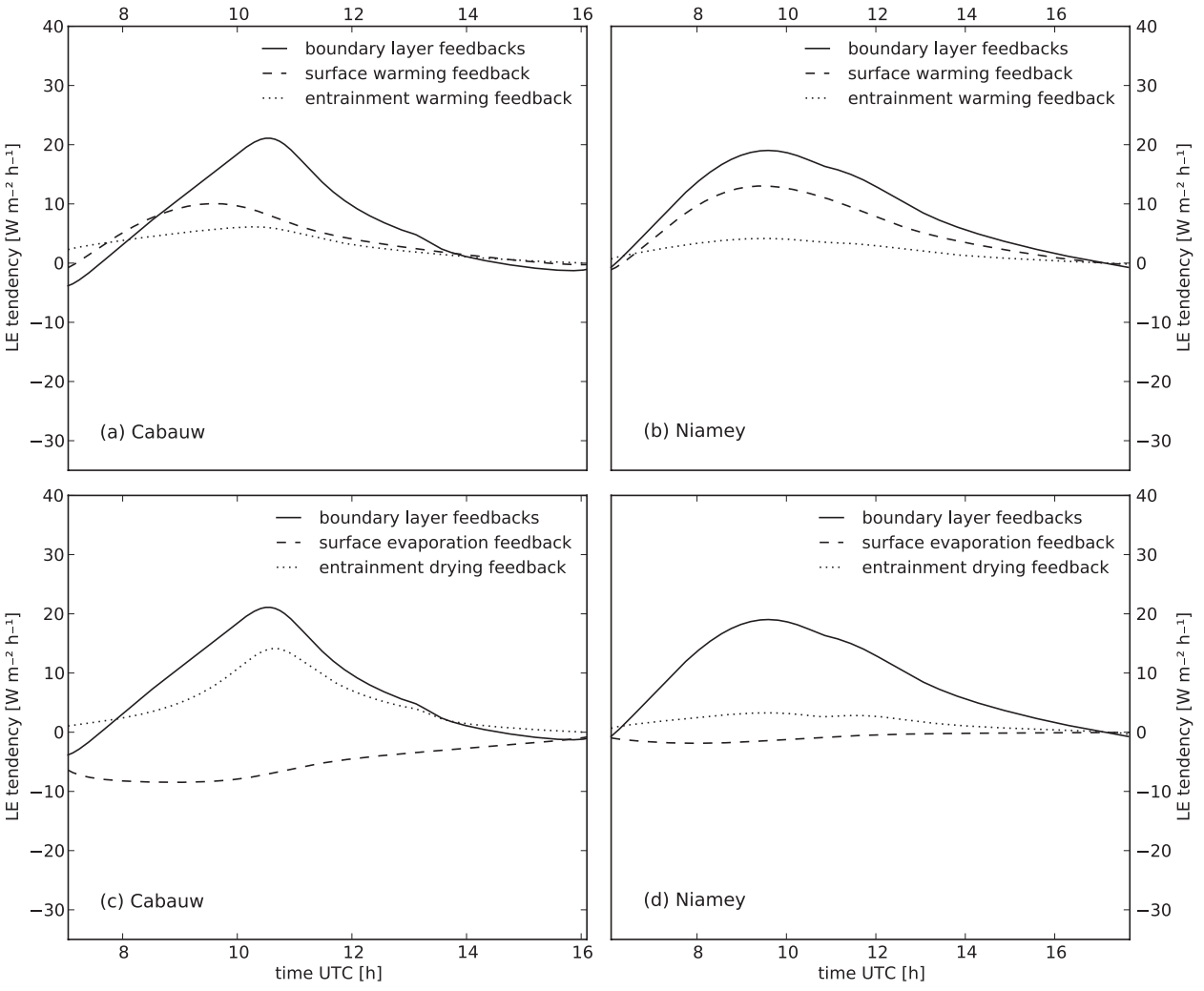

FIG. 8. Contributions to the tendency of the surface evaporation induced by boundary layer temperature feedbacks for (top left) Cabauw and (top right) Niamey and boundary layer humidity feedbacks for (bottom left) Cabauw and (bottom right) Niamey.

the day than moisture entrainment and is, except for the early morning, smaller in magnitude than the surface sensible heat flux.

At Niamey, the boundary layer feedbacks are mostly controlled by temperature. The surface warming feedback contributes up to 13 W m^{-2} h^{-1} to the time evolution, whereas the other three feedbacks have only a limited influence ranging from -2 W m^{-2} h^{-1} for the surface evapotranspiration to $\sim$3 W m^{-2} h^{-1} for both entrainment fluxes.

The differences between the boundary layer feedbacks at Cabauw and Niamey have two reasons. First, the evapotranspiration flux is smaller at Niamey. Therefore, the opportunity for evapotranspiration to moisten the atmosphere to influence evapotranspiration significantly is limited. Nevertheless, there is large dry-air entrainment flux at Niamey; thus, we need another explanation for the low sensitivity of the evapotranspiration to dry air. The answer is in the nonlinear relationship between saturated specific humidity and temperature, described by the Clausius–Clapeyron relationship plotted in Fig. 9. If the temperature is relatively low, such as at Cabauw, then variations in the moisture deficit $q_{sat} - q$ are just as dependent on variations in temperature as on variations in moisture. For conditions of higher temperatures, however, the saturated specific humidity is much more sensitive to variations at high temperature than at low temperature. Therefore, variations in the moisture deficit are mainly caused by variations in temperature. For example, at Cabauw, q_{sat} changes from 10.0 to 12.3 g kg^{-1} between 1000 and 1500 UTC (see Fig. 9), whereas q changes from 5.6 to 4.9. At Niamey, however, q_{sat} increases from 27.4 to 38.0 g kg^{-1} between 1000 and 1500 UTC (see Fig. 9), whereas q only decreases from

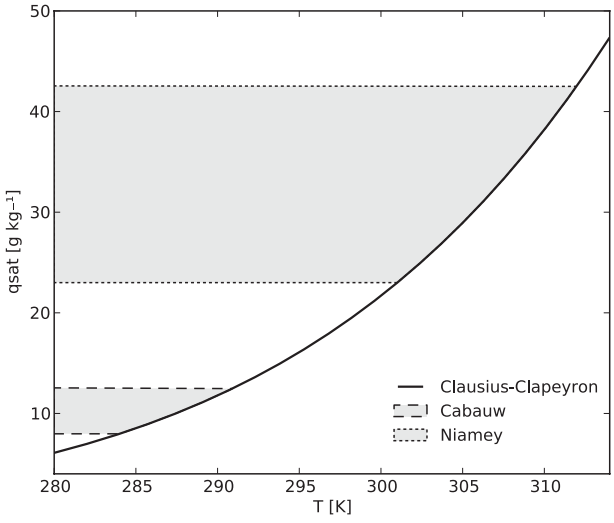

FIG. 9. Comparison of the daily range of q_{sat} at Cabauw (dashed lines) and Niamey (dotted lines) indicated as the Clausius–Clapeyron relationship between absolute temperature and saturated specific humidity.

13.5 to 10.9 g kg^{-1}. From this analysis, we can conclude that due to the nonlinear relation between temperature and saturated humidity, dry-air entrainment is particularly significant at lower temperatures. These observed cases thus confirm the theoretical experiments of van Heerwaarden et al. (2009), who showed that the impact of dry-air entrainment becomes less at higher temperatures. Our finding also extends to previous studies on the effect of dry-air entrainment in the Sahel region (Lothon et al. 2007; Canut et al. 2010), by showing that dry air only has a minimal impact on the surface heat fluxes, despite its large impact on the specific humidity and thus on cloud formation and convection. In between these two regimes, there is a gradual transition from one regime into the other. This becomes clear in the results of Margulis and Entekhabi (2001), who analyzed a case in which the temperature is significantly higher than at Cabauw, but less than at Niamey, while the Bowen ration resembles that of the Cabauw case. In their results, the sensitivity of evapotranspiration to the free atmospheric humidity is less than in our Cabauw case, and less than the impact of temperature on evaporation, but it is clearly larger than the impact of free atmospheric humidity in the Niamey case.

Returning to the question why the boundary layer feedbacks are so similar between the two cases, it is coincidental as an in-depth analysis shows there are significant differences between the four contributions of the boundary layer feedbacks.

4) FORCINGS

In Fig. 10 we give an overview of the forcings of the coupled land–atmosphere system in the two cases. This figure completes the overview of all the terms in Eq. (1). In both cases the total forcings are mainly depending on the contribution of incoming shortwave radiation since both curves in the figure nearly overlap. In section 4b(1) we found that the impact of the forcings decreases in the afternoon at Niamey, while this is not the case at Cabauw. The explanation for this is related to the difference in land surface feedbacks discussed in section 4b(2). Owing to drying of the soil and the subsequent increase in surface resistance, the evaporation is strongly limited by the land

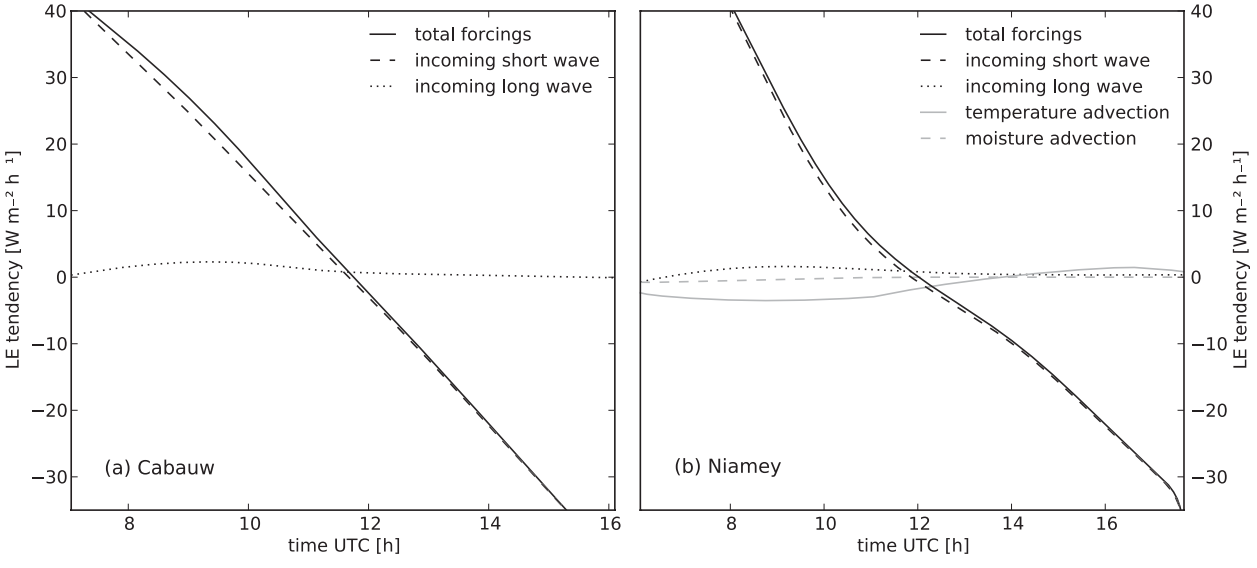

FIG. 10. Contributions of the forcings to the tendency of the surface evaporation for (left) Cabauw and (right) Niamey.

surface conditions. The response of the evapotranspiration to falling radiation is therefore limited since at this time the case is fully water limited and radiation is no longer a limiting factor for evapotranspiration.

Based on this figure, we can argue that our assumption that the incoming longwave radiation is an external forcing is correct. In both situations the daily dynamics of the atmospheric temperature barely influence the impact of the incoming longwave radiation.

There is one extra feature in the forcings at Niamey, which is the large-scale advection of moist and cold air. This gradually decreasing advection has a slight negative impact on evapotranspiration. Initially, the temperature advection has an impact of -3 W m^{-2} h^{-1}, which gradually increases to 0 W m^{-2} h^{-1}. The moisture advection does not exert any influence at all. The explanation is similar to that of the insensitivity of evapotranspiration to dry-air entrainment at high temperatures: the moisture deficit is largely determined by temperature variations and only little by variations in specific humidity.

5. Conclusions

A method to analyze the daily cycle of surface evapotranspiration has been developed. It reveals novel insight on the driving mechanisms behind surface evapotranspiration during the day. The method shows clearly that surface evapotranspiration is a complex process that can only be understood by considering the land surface and the atmosphere as an interactive system. It quantifies separately variations in the surface evapotranspiration driven by direct forcings, such as radiation, as well as those driven by feedbacks that exist between evapotranspiration and the land surface, the surface layer, and the atmospheric boundary layer (ABL).

We modeled and validated with data two contrasting observed cases: 25 September 2003 at Cabauw, Netherlands, and 22 June 2006, at Niamey, Niger. The first case is a characteristic example of a case in which evapotranspiration is energy limited, whereas the second is a typical water-limited case. Subsequently, we apply our method to the model output. This reveals insights into the mechanisms that drive evapotranspiration at these locations.

We find that forcings and feedbacks are of equal importance in the control of surface evapotranspiration. The local conditions determine how much the feedbacks enhance or suppress the forcings. At Cabauw, the feedbacks enhance evapotranspiration because their sum is positive over the majority of the day. At Niamey the opposite is true: here the sum of the feedbacks is mostly negative, which indicates that evapotranspiration is suppressed by the land–atmosphere system. In both cases the boundary layer feedbacks, the effects of changes in the temperature and moisture content of the ABL, have an enhancing effect on evapotranspiration. In the case of Niamey, this effect is offset by the strong negative influence of the land surface feedbacks, induced by drying of the soil.

Despite the similarity in the sign and magnitude of the boundary layer feedbacks in both cases, there is a large difference in the processes that drive them. In the case of Cabauw, the variations of moisture and temperature in the atmosphere play an equally important role, and dry-air entrainment has the largest contribution to the boundary layer feedbacks. At Niamey, however, the effect of temperature fluctuations dominates the feedbacks and moisture fluctuations become irrelevant. In general, it should be true that over cold areas in the world, both atmospheric moisture and temperature regulate the boundary layer feedbacks. If we move toward regions with high temperatures, we expect a gradual transition toward a regime where the boundary layer feedbacks become temperature controlled.

Although our method shows interesting features of the diurnal cycle of evapotranspiration, we would like to stress that our conclusions are only based on two cases that mainly served as examples of our new method. To acquire a solid understanding of the driving forces behind the daily cycle of evapotranspiration, future studies that take into account longer time periods and more locations are necessary. Such studies could enable us to identify for different areas in the world to which changes in the environment the evapotranspiration would be the most sensitive and how this sensitivity varies in space and time. This could for instance be done using output of weather and climate models. Before such studies can be undertaken, our model needs to be extended to cloudy boundary layers.

Acknowledgments. The first author acknowledges Météo-France for supporting his research visit. This study was supported by a grant from the Netherlands Organization for Scientific Research (NWO TopTalent). The authors acknowledge the Royal Netherlands Meteorological Institute (KNMI) and Fred Bosveld for making the Cabauw data available.

APPENDIX A

Derivation of the Evapotranspiration Tendency Equation

In this appendix we derive the tendency equation for evapotranspiration from the Penman–Monteith equation

and the mixed-layer equations that describe the daytime ABL:

$$LE = \frac{\frac{dq_{\mathrm{sat}}}{dT}(Q_* - G) + \frac{\rho c_p}{r_a}(q_{\mathrm{sat}} - q)}{\frac{dq_{\mathrm{sat}}}{dT} + \frac{c_p}{L_v}\left(1 + \frac{r_s}{r_a}\right)}. \quad \text{(A1)}$$

The Penman–Monteith equation [Eq. (A1)] describes the actual evapotranspiration taking into account all processes that create a moisture gradient between the land surface and the atmosphere. These are the available energy, defined as the net radiation Q_* minus the soil heat flux G, and the moisture deficit of the air, which is the saturated specific humidity of the atmosphere q_{sat} minus its specific humidity q. The extent to which moisture can be transported over this gradient is determined by the turbulence near the surface, described by the aerodynamic resistance r_a, and the ability of the vegetation and soil to evaporate water, described by the surface resistance r_s. Note that the terms in the equation are in units of specific humidity rather than the more commonly used vapor pressure to facilitate the coupling with our atmospheric model.

If we differentiate this expression in time and group all terms in the equation per the tendency of each of the involved variables and finally replace $Q_* - G - LE$ by H, we obtain Eqs. (A2) and (A3):

$$c_0 = 1 \Big/ \left[\frac{dq_{\mathrm{sat}}}{dT} + \frac{c_p}{L_v}\left(1 + \frac{r_s}{r_a}\right)\right] \quad \text{(A2)}$$

and

$$\frac{dLE}{dt} = c_0 \frac{dq_{\mathrm{sat}}}{dT}\frac{dQ*}{dt} - c_0 \frac{dq_{\mathrm{sat}}}{dT}\frac{dG}{dt} + c_0\left(H\frac{d^2 q_{\mathrm{sat}}}{dT^2} + \frac{\rho c_p}{r_a}\frac{dq_{\mathrm{sat}}}{dT}\right)\frac{dT}{dt} - c_0\frac{\rho c_p}{r_a}\frac{dq}{dt} - c_0\left(\frac{\rho c_p}{r_a^2}(q_{\mathrm{sat}} - q) - LE\frac{c_p}{L_v}\frac{r_s}{r_a^2}\right)\frac{dr_a}{dt} - c_0 LE\frac{c_p}{L_v}\frac{1}{r_a}\frac{dr_s}{dt}. \quad \text{(A3)}$$

With the previous equation, we have decomposed the evolution of evaporation in one term per involved variable. Nevertheless, the tendency of each variable is also the sum of a set of physical processes. We elaborate now on some of the terms to improve the physical interpretation.

First, we split the net radiation tendency into the sum of the tendencies of the net shortwave and longwave radiation:

$$\frac{dQ_*}{dt} = (1 - \alpha)\frac{dS_{\mathrm{in}}}{dt} + \frac{dL_{\mathrm{in}}}{dt} - \frac{dL_{\mathrm{out}}}{dt}, \quad \text{(A4)}$$

where α is the albedo, S_{in} is the incoming shortwave radiation at the surface, L_{in} is the incoming longwave radiation at the surface, and L_{out} is the outgoing longwave radiation at the surface.

Second, we introduce the essential dynamics of the atmosphere into the temperature and moisture equation. Previous studies (Betts 1992; Santanello et al. 2009) show that the time evolution of the near-surface temperature and humidity is the effect of both external forcings such as advection and radiation divergence, as well as internal feedbacks such as the surface fluxes of heat and moisture and the entrainment fluxes of heat and moisture, which is the interaction between the turbulent boundary layer and the free atmosphere above.

During daytime, the effects of the large-scale forcings and feedbacks are rapidly mixed throughout the atmospheric boundary layer. Therefore, the layer can be considered as well mixed and one value of the conserved variables, specific humidity and potential temperature, is representative for that layer. This yields the widely applied mixed layer model (Lilly 1968; Tennekes 1973):

$$w_e = A_{\theta_v}\left[\frac{H}{\rho c_p} + \theta\left(\frac{R_v}{R_d} - 1\right)\frac{LE}{\rho L_v}\right] \Big/ \Delta\theta_v, \quad \text{(A5)}$$

$$\frac{dh}{dt} = w_e + w_s, \quad \text{(A6)}$$

$$\frac{d\theta}{dt} = \frac{1}{h}\left(\frac{H}{\rho c_p} + w_e\Delta\theta\right) + \mathrm{adv}_\theta, \quad \text{(A7)}$$

$$\frac{dq}{dt} = \frac{1}{h}\left(\frac{LE}{\rho L_v} + w_e\Delta q\right) + \mathrm{adv}_q, \quad \text{(A8)}$$

$$\frac{d\Delta\theta}{dt} = \gamma_\theta\frac{dh}{dt} - \frac{d\theta}{dt}, \quad \text{(A9)}$$

and

$$\frac{d\Delta q}{dt} = \gamma_q\frac{dh}{dt} - \frac{dq}{dt} \quad \text{(A10)}$$

in which w_e is the entrainment velocity, A_{θ_v} the ratio between the entrainment virtual heat flux and the surface virtual heat flux, ρ the density of air, c_p the heat

TABLE C1. Initial and boundary conditions for model runs 25 Sep 2003 at Cabauw and 22 Jun 2006 at Niamey, without those for the mixed-layer, which are in Table 2.

Variable	Description and unit	Cabauw	Niamey
P_0	Surface pressure (Pa)	102 900.00	98 500.00
w_s	Large-scale vertical velocity (m s^{-1})	0.0	0.0
lat	Latiutde (°)	51.97°N	13.48°N
lon	Longitude (°)	4.93°E	2.17°E
doy	Day of the year (−)	268.00	173.00
w_g	Volumetric water content top soil layer (m^3 m^{-3})	0.43	0.198
w_2	Volumetric water content deeper soil layer (m^3 m^{-3})	0.43	0.20
c_{veg}	Vegetation fraction (−)	0.9	0.2
T_{soil}	Temperature top soil layer (K)	282.00	300.00
T_2	Temperature deeper soil layer (K)	285.00	290.00
a	Clapp–Hornberger retention curve parameter (−)	0.083	0.219
b	Clapp–Hornberger retention curve parameter (−)	11.4	4.90
p	Clapp–Hornberger retention curve parameter (−)	12.00	4.00
CG_{sat}	Saturated soil conductivity for heat (K m^{-2} J^{-1})	3.6×10^{-6}	3.56×10^{-6}
w_{sat}	Saturated volumetric water content (m^3 m^{-3})	0.600	0.472
w_{fc}	Volumetric water content field capacity (m^3 m^{-3})	0.491	0.323
w_{wilt}	Volumetric water content wilting point (m^3 m^{-3})	0.314	0.171
$C1_{sat}$	Coefficient force term moisture (−)	0.342	0.132
$C2_{ref}$	Coefficient restore term moisture (−)	0.3	1.8
LAI	Leaf area index of vegetated surface fraction (−)	2.00	2.00
$r_{c,min}$	Minimum resistance transpiration (s m^{-1})	110.00	110.00
$r_{s,soil,min}$	Minimum resistance soil evaporation (s m^{-1})	50.00	50.00
g_D	VPD correction factor for surface resistance (−)	0.00	0.00
z_{0m}	Roughness length for momentum (m)	0.05	0.05
z_{0h}	Roughness length for heat and moisture (m)	0.01	0.01
α	Surface albedo (−)	0.25	0.21
W_l	Equivalent water layer depth for wet vegetation (m)	1.4×10^{-4}	0.0

capacity of air at constant pressure, R_v the gas constant of moist air, R_d the gas constant of dry air, and w_s is the large-scale vertical motion.

The most important assumptions that are enclosed in this model are the following.

- The ABL is well mixed: therefore, one value for the potential temperature and specific humidity is used for the whole layer (see sketch of vertical profiles in Fig. 1).
- The boundary layer growth [see Eq. (A6)] is driven by the large-scale vertical velocity w_s and the surface virtual potential temperature flux [see Eq. (A5)] where this value is written in terms of the heat fluxes. The entrainment parameter A_{θ_v} relates the entrainment flux of virtual potential temperature to the surface flux. The entrainment zone is assumed to be of infinitesimal thickness (see sketch of vertical profiles in Fig. 1).
- The prognostic equations for the jumps of potential temperature and specific humidity between the ABL and the free atmosphere [see Eqs. (A9) and (A10)] show that the jump is a competition of boundary layer growth and the time evolution of the mixed-layer values of potential temperature [see Eq. (A7)] and specific humidity [see Eq. (A8)].

A complete description of all the physical assumptions behind the model can be found in Tennekes (1973).

Equations (A7) and (A8) are used to replace the temperature and moisture tendencies in Eq. (A3), thereby assuming that at the land surface the absolute temperature and the potential temperature are equal.

APPENDIX B

Detailed Description of the Jarvis–Stewart Model

In our model the surface resistance r_s is modeled using a Jarvis–Stewart model with the following specifications:

$$r_s = \frac{r_{s,\min}}{\mathrm{LAI}} f_1(S_{\mathrm{in}}) f_2(w) f_3(\mathrm{VPD}) f_4(T) \qquad \text{(B1)}$$

in which $r_{s,min}$ is the minimum surface resistance, LAI the leaf area index of the vegetated fraction, f_1 a correction function depending on incoming shortwave radiation S_{in}, f_2 a function depending on soil moisture w, f_3 a function depending on vapor pressure deficit VPD, and f_4 is a function depending on temperature T.

The correction functions, of which the first three are taken from the ECMWF IFS and the fourth from Noilhan and Planton (1989), are

TABLE C2. Mixed-layer initial and boundary conditions of model runs of 25 Sep 2003 at Cabauw and 22 Jun 2006 at Niamey.

Variable	Description and unit	Cabauw	Niamey
h	Initial ABL height (m)	175.00	400.00
θ	Initial mixed-layer potential temperature (K)	284.5	301.2
$\Delta\theta$	Initial temperature jump h (K)	4.2	3.6
γ_θ	Potential temperature lapse rate (K m^{-1})	$0.0036_{h\leq 950\text{m}}$	$0.010_{h\leq 700\text{m}}$
		$0.015_{h>950\text{m}}$	$0.0034_{h>700\text{m}}$
A_{θ_v}	Entrainment ratio virtual potential temperature (−)	0.3	0.18
adv_θ	Advection of heat (K s^{-1})	0.00	$f_\theta(t)$
q	Initial mixed-layer specific humidity (kg kg^{-1})	0.0044	0.0138
Δq	Initial specific humidity jump at h (kg kg^{-1})	-8.0×10^{-4}	−0.0044
γ_q	Specific humidity lapse rate (kg kg^{-1} m^{-1})	-1.2×10^{-6}	-1.4×10^{-6}
adv_q	Advection of moisture (kg kg^{-1} s^{-1})	0.00	$f_q(t)$
u	Initial mixed-layer wind speed (m s^{-1})	5.00	5.00
Δu	Initial momentum jump at h (m s^{-1})	3.00	0.00
γ_u	Free atmosphere wind speed lapse rate (s^{-1})	0.002	0.001
$f_\theta(t)$	-1.0×10^{-4} (K s^{-1})$_{t\leq 11\text{hUTC}}$		
	-1.0×10^{-4} max[1.00 − 0.36 ($t_{\text{hUTC}} - 6$), −1] (K s^{-1})$_{t>11\text{hUTC}}$		
$f_q(t)$	4.17×10^{-8} max[1.00 − 0.18 ($t_{\text{hUTC}} - 6$), 0] (kg kg^{-1} s^{-1})$_{t\leq 11\text{hUTC}}$		

$$\frac{1}{f_1(S_{\text{in}})} = \min\left(1, \frac{0.004S_{\text{in}} + 0.05}{0.81(0.004S_{\text{in}} + 1)}\right), \tag{B2}$$

$$\frac{1}{f_2(w)} = \frac{w - w_{\text{wilt}}}{w_{\text{fc}} - w_{\text{wilt}}}, \tag{B3}$$

$$\frac{1}{f_3(VPD)} = \exp(g_D \text{VPD}), \tag{B4}$$

and

$$\frac{1}{f_4(T)} = 1.0 - 0.0016(298.0 - T)^2, \tag{B5}$$

where w_{wilt} is the volumetric soil moisture at wilting point, w_{fc} is the volumetric soil moisture at field capacity, and g_D is a correction factor for vapor pressure deficit.

APPENDIX C

Initial and Boundary Conditions Coupled Model

Tables C1 and C2 show the initial and boundary conditions for the two cases.

REFERENCES

Betts, A. K., 1992: FIFE atmospheric boundary layer budget methods. *J. Geophys. Res.,* **97,** 18 525–18 531.

——, J. H. Ball, A. C. M. Beljaars, M. J. Miller, and P. A. Viterbo, 1996: The land surface–atmosphere interaction: A review based on observational and global modeling perspectives. *J. Geophys. Res.,* **101,** 7209–7225.

Brotzge, J. A., and K. C. Crawford, 2003: Examination of the surface energy budget: A comparison of eddy correlation and Bowen ratio measurement systems. *J. Hydrometeor.,* **4,** 160–178.

Brubaker, K. L., and D. Entekhabi, 1995: An analytic approach to land–atmosphere interaction: 1. Construct and equilibrium behavior. *Water Resour. Res.,* **31,** 619–632.

——, and ——, 1996: Analysis of feedback mechanisms in land–atmosphere interaction. *Water Resour. Res.,* **32,** 1343–1357.

Canut, G., M. Lothon, F. Saïd, and F. Lohou, 2010: Observation of entrainment at the interface between monsoon flow and the Saharan air layer. *Quart. J. Roy. Meteor. Soc.,* **136,** 34–46, doi:10.1002/qj.471.

Casso-Torralba, P., J. Vilà-Guerau de Arellano, F. Bosveld, M. R. Soler, A. Vermeulen, C. Werner, and E. Moors, 2008: Diurnal and vertical variability of the sensible heat and carbon dioxide budgets in the atmospheric surface layer. *J. Geophys. Res.,* **113,** D12119, doi:10.1029/2007JD009583.

De Bruin, H. A. R., 1983: A model for the Priestley–Taylor parameter α. *J. Climate Appl. Meteor.,* **22,** 572–578.

Duynkerke, P. G., 1991: Radiation fog: A comparison of model simulation with detailed observations. *Mon. Wea. Rev.,* **119,** 324–341.

Ek, M. B., and A. A. M. Holtslag, 2004: Influence of soil moisture on boundary layer cloud development. *J. Hydrometeor.,* **5,** 86–99.

Jacobs, C. J. M., and H. A. R. De Bruin, 1992: The sensitivity of regional transpiration to land–surface characteristics: Significance of feedback. *J. Climate,* **5,** 683–698.

Jarvis, P. G., 1976: The interpretation of the variations in leaf water potential and stomatal conductance found in canopies in the field. *Philos. Trans. Roy. Soc. London,* **B273,** 593–610.

Koster, R. D., and Coauthors, 2004: Regions of strong coupling between soil moisture and precipitation. *Science,* **305,** 1138–1140, doi:10.1126/science.1100217.

Lilly, D. K., 1968: Models of cloud-topped mixed layers under a strong inversion. *Quart. J. Roy. Meteor. Soc.,* **94,** 292–309.

Lothon, M., F. Couvreux, S. Donier, F. Guichard, P. Lacarrère, D. H. Lenschow, J. Noilhan, and F. Saïd, 2007: Impact of coherent eddies on airborne measurements of vertical turbulent fluxes. *Bound.-Layer Meteor.,* **124,** 425–447, doi:10.1007/s10546-007-9182-9.

Margulis, S. A., and D. Entekhabi, 2001: Feedback between the land surface energy balance and atmospheric boundary layer diagnosed through a model and its adjoint. *J. Hydrometeor.,* **2,** 599–620.

McNaughton, K. G., and T. W. Spriggs, 1986: A mixed-layer model for regional evaporation. *Bound.-Layer Meteor.,* **34,** 243–262.

Miller, M. A., and A. Slingo, 2007: The ARM mobile facility and its first international deployment: Measuring radiative flux divergence in West Africa. *Bull. Amer. Meteor. Soc.,* **88,** 1229–1244.

Monteith, J. L., 1965: Evaporation and environment. *Symp. Soc. Exp. Biol.,* **19,** 205–234.

Noilhan, J., and S. Planton, 1989: A simple parameterization of land surface processes for meteorological models. *Mon. Wea. Rev.,* **117,** 536–549.

Paulson, C. A., 1970: The mathematical representation of wind speed and temperature profiles in the unstable atmospheric surface layer. *J. Appl. Meteor.,* **9,** 857–861.

Ramier, D., and Coauthors, 2009: Towards an understanding of coupled physical and biological processes in the cultivated Sahel—1. Energy and water. *J. Hydrol.,* **375,** 204–216.

Raupach, M. R., 2000: Equilibrium evaporation and the convective boundary layer. *Bound.-Layer Meteor.,* **96,** 107–141.

Redelsperger, J. L., C. D. Thorncroft, A. Diedhiou, T. Lebel, D. J. Parker, and J. Polcher, 2006: African monsoon multidisciplinary analysis: An international research project and field campaign. *Bull. Amer. Meteor. Soc.,* **87,** 1739–1746.

Santanello, J. A., M. A. Friedl, and M. B. Ek, 2007: Convective planetary boundary layer interactions with the land surface at diurnal time scales: Diagnostics and feedbacks. *J. Hydrometeor.,* **8,** 1082–1097.

——, C. D. Peters-Lidard, S. V. Kumar, C. Alonge, and W.-K. Tao, 2009: A modeling and observational framework for diagnosing local land–atmosphere coupling on diurnal time scales. *J. Hydrometeor.,* **10,** 577–599.

Sellers, P. J., F. G. Hall, G. Asrar, D. E. Strebel, and R. E. Murphy, 1992: An overview of the First International Satellite Land Surface Climatology Project (ISLSCP) Field Experiment (FIFE). *J. Geophys. Res.,* **97,** 18 345–18 371.

Steeneveld, G. J., B. J. H. van de Wiel, and A. A. M. Holtslag, 2007: Diagnostic equations for the stable boundary layer height: Evaluation and dimensional analysis. *J. Appl. Meteor. Climatol.,* **46,** 212–225.

Tennekes, H., 1973: A model for the dynamics of the inversion above a convective boundary layer. *J. Atmos. Sci.,* **30,** 558–567.

van Heerwaarden, C. C., J. Vilà-Guerau de Arellano, A. F. Moene, and A. A. M. Holtslag, 2009: Interactions between dry-air entrainment, surface evaporation and convective boundary-layer development. *Quart. J. Roy. Meteor. Soc.,* **135,** 1277–1291, doi:10.1002/qj.431.

Viterbo, P., and A. C. M. Beljaars, 1995: An improved land surface parameterization scheme in the ECMWF model and its validation. *J. Climate,* **8,** 2716–2748.